Published in final edited form as:
*IEEE J Quantum Electron*. 2011 ; 47(5): 597–606. doi:10.1109/JQE.2011.2107730.

# Scaling Fiber Lasers to Large Mode Area: An Investigation of Passive Mode-Locking Using a Multi-Mode Fiber

**Edwin Ding**,
Department of Applied Mathematics, University of Washington, Seattle, WA 98195 USA

**Simon Lefrancois**,
Department of Applied Physics, Cornell University, Ithaca, NY 14853 USA

**Jose Nathan Kutz**, and
Department of Applied Mathematics, University of Washington, Seattle, WA 98195 USA

**Frank W. Wise**
Department of Applied Physics, Cornell University, Ithaca, NY 14853 USA

Edwin Ding: ding@amath.washington.edu; Simon Lefrancois: sl694@cornell.edu; Jose Nathan Kutz: kutz@amath.washington.edu; Frank W. Wise: fwise@ccmr.cornell.edu

## Abstract

The mode-locking of dissipative soliton fiber lasers using large mode area fiber supporting multiple transverse modes is studied experimentally and theoretically. The averaged mode-locking dynamics in a multi-mode fiber are studied using a distributed model. The co-propagation of multiple transverse modes is governed by a system of coupled Ginzburg–Landau equations. Simulations show that stable and robust mode-locked pulses can be produced. However, the mode-locking can be destabilized by excessive higher-order mode content. Experiments using large core step-index fiber, photonic crystal fiber, and chirally-coupled core fiber show that mode-locking can be significantly disturbed in the presence of higher-order modes, resulting in lower maximum single-pulse energies. In practice, spatial mode content must be carefully controlled to achieve full pulse energy scaling. This paper demonstrates that mode-locking performance is very sensitive to the presence of multiple waveguide modes when compared to systems such as amplifiers and continuous-wave lasers.

### Index Terms

Large mode area fibers; mode-locked lasers; multi-mode fibers; solitons

## I. INTRODUCTION

Over the past two decades, mode-locked lasers have evolved from the confines of fundamental science to commercial instruments with a wide variety of applications [1], [2]. Currently there is a high level of interest in mode-locked fiber lasers due to the practical advantages they offer over solid-state lasers. Despite much progress in mode-locked fiber lasers, their broader impact has been limited due to restrictions on pulse energies, which is a consequence of the underlying soliton area theorem [1]. Thus the standard and well-known multi-pulsing instability [1], [3]–[6] prevents the formation of highly-energetic pulses. Indeed, conventional soliton fiber lasers [7] that rely on the balance between anomalous group velocity dispersion (GVD) and self-phase modulation (SPM) only generate pulses with energies up to ~0.1 nJ [1], [2]. Recently, much progress has been made experimentally to achieve higher energy mode-locked fiber lasers by using segments of normal GVD fiber so that the net cavity dispersion is near zero or large and normal. These include the

stretched-pulse laser [8]–[10], self-similar laser [2], [11], and the all-normal dispersion (ANDi) laser [2], [12]–[15]. When combined with large mode area (LMA) fibers, ANDi lasers have recently produced pulses with peak powers at the megawatt level [15]–[17]. In contrast to soliton mode-locked lasers [1], [7], this new generation of high power fiber lasers depend strongly on dissipative processes as well as phase modulations to shape the pulse, often resulting in large intra-cavity pulse variations per round trip. Although these dissipative solitons [14] tolerate nonlinear phase shifts up to ~10π, the build-up of a strong enough nonlinear phase shift still induces a multi-pulsing instability in these fiber lasers. An area theorem for dissipative solitons has been derived [18], with energy limits at least two orders of magnitude above conventional soliton lasers for given mode area.

To further increase mode-locked pulse energies, the fiber nonlinearity must be reduced in order to avoid multi-pulsing. A conceptually-straightforward way to further increase the power levels in a laser cavity is by using fibers with larger cores, increasing the pulse energy while maintaining the nonlinear phase shift incurred. This approach is limited, however, by the potential onset of multimode waveguiding. The transition from single-mode to multi-mode operation for step-index fiber can be easily computed [19], thus giving a maximal core radius for single-mode operation. The lowest-order mode of a multimode fiber can have large area, and use of multimode fiber in this way has become a popular and practical means of achieving large mode area. Several mechanisms have been demonstrated to filter out higher-order modes, including selective bend loss [20], gain filtering [21], and chirally-coupled core (CCC) fiber [22]. Photonic-crystal fiber (PCF) allows large effectively single-mode core, either due to large propagation losses for higher-order modes, or weak intermodal coupling. The use of PCF has been popular in scientific studies, but has had less impact in practical devices due to high bend sensitivity and difficult integration with conventional fiber fusion technology. Step index multi-mode fibers offer straightforward integration potential. Although they have found wide use in amplifiers, there has only been one isolated demonstration of their use in mode-locked oscillators [23]. It is suspected that interaction with higher-order modes (HOM) may disrupt stable mode-locking in laser cavities.

One of the most successful mode-locked lasers developed to date is the ring cavity fiber laser with passive polarizer and waveplate elements [1], [3], [24]–[26]. The combination of these passive mode-locking elements creates the self-amplitude modulation, which is generated by Kerr-lensing [27], [28] or a saturable absorber in solid-state lasers. Such a mode-locking technique is in general referred to as nonlinear polarization rotation or evolution (NPE), although other physical mechanisms such as nonlinear interferometry [29]–[32], active modulation [33], [34], or nonlinear mode-coupling [35]–[38] can also be used to achieve effective intensity discrimination. The best-known theoretical model used to describe the averaged mode-locking process in ring cavity fiber lasers is the master equation proposed by H. A. Haus, which is essentially the cubic complex Ginzburg-Landau equation [1]. A quintic absorption term is commonly added to the master equation to capture the robust nature of the experimentally observed mode-locking process [3], [39], [40]. Recently, Leblond *et al.* [26], [41], [42] and Ding and Kutz [43] have developed split-step modeling techniques to average the pulse propagation in the cavity subjected to the discrete effects of the passive polarizer and wave-plates. This resulted in an cubic-quintic complex Ginzburg-Landau equation where all the coefficients in the equation could be explicitly related to the settings of the discrete elements. However, this model is only applicable to lasers built with single-mode fiber. The coupled mode theory describes the co-propagation of different fiber modes in a multi-mode fiber which is governed by a set of coupled nonlinear Schrödinger equations (CNLS), and has been considered in numerous earlier works [19], [44]–[48]. However the pulse shaping mechanism, i.e. the effective saturable absorption created by the wave-plates and polarizer, is not incorporated into the governing equation.

In this work, we investigate theoretically and experimentally the possibility of mode-locked operation of an ANDi fiber laser based on large core fibers supporting multiple transverse modes. Theoretically, we extend the coupled mode theory derived by Kutz and co-workers [44] to account explicitly for the effects of saturable absorption as well as gain saturation, thus resulting in a system of coupled complex Ginzburg-Landau equations (CGLEs) with cubic-quintic dissipation. Thus, we explicitly consider the multi-mode dynamics due to nonlinear mode coupling in the laser cavity and show that stable mode-locking is indeed achievable. We use this model to study the destabilizing effect of multimode propagation on achievable mode-locked pulse energies, as well as the beneficial effects of mode filtering. The coupled CGLE model considered in this paper is, to our knowledge, the first theoretical model that treats the averaged evolution in multi-mode fiber lasers and explicitly accounts for saturable absorption as well as the stabilizing effect of gain saturation [43], [49], [50]. Experimentally, we find that the presence of unsuppressed higher order mode content in LMA fibers significantly reduces the maximum single pulse energy that can be stabilized in the cavity, confirming the destabilizing effect of multimode propagation. Careful control of higher-order mode content can restore full pulse energy scaling. This is shown in the case of step-index fiber, large core photonic crystal fiber, as well as chirally-coupled core fiber.

The paper is structured as follows: Sec. II describes the extended coupled mode theory that describes the averaged pulse evolution in a generic multi-mode ring cavity fiber laser. Extensive numerical simulations showing the mode-locking behavior as a function of the key physical parameters in the laser cavity are given in Sec. III. The experimental realization of the laser cavities and their behavior is given in Sec. IV. Sec. V concludes the paper with a summary of results and highlights the key findings related to the multi-mode operation of fiber lasers.

## II. COUPLED MODE THEORY AND AVERAGE LASER CAVITY DYNAMICS

The theoretical underpinnings of a multi-mode model are presented in this section. Critical in a quantitative description is a fundamental characterization of the nonlinear mode-coupling which occurs between the fundamental mode and the second mode of the fiber. A higher number of modes can be incorporated into the model developed here, but simulations show that the two-mode case exhibits the key features of a multi-mode laser. Although the model is constrained to a two-mode analysis, the general trends presented here hold even in the presence of higher-order mode content. Thus the two-mode model elucidates the essential features of the multi-mode mode-locking and instability.

### A. Fiber Modes

Fig. 1 shows the idealized ring cavity laser consisted of a single-mode fiber (SMF) in conjunction with an ytterbium-doped multi-mode fiber (MMF), a saturable absorber (a combination of wave-plates and polarizers), and an output coupler. For the rest of Secs. II and III, we will treat the entire laser cavity as one single MMF. This is consistent with experiment (See Fig. 8) as the SMF is short (≈ 30% of the total cavity length), and it is only used to control the mode excitation in the MMF. This modal excitation however, only affects the initial second mode content created at each roundtrip, not the pulse propagation in the system. The effects of bandwidth-limited Yb-doped amplification, fiber losses, and saturable absorption will be treated with a distributed model so that they are distributed along the entire cavity length [1], [3].

The derivation of the transverse mode fields supported by the multi-mode fiber and the corresponding envelope equations has been considered in earlier works [19], [44]–[48], and hence we will only highlight the key results here. It has been shown [19] that the mode

fields $\Psi_j$ ($j = 1, \ldots, N$, where $N$ is the total number of modes) supported by the multi-mode fiber satisfy the eigenvalue problem

$$\nabla_\perp^2 \Psi_j + \left(k^2 n^2(x,y) - \Lambda_j^2\right) \Psi_j = 0, \tag{1}$$

where $\nabla_\perp^2 = \partial_x^2 + \partial_y^2$ is the transverse Laplacian, $k = 2\pi/\lambda$ is the wave number in the propagation direction $z$, $n(x, y)$ is the effective refractive index profile of the fiber's cross-section, and $\Lambda_j$ is the propagation constant (eigenvalue) of the $j^{th}$ mode. As a leading-order approximation, only radially symmetric modes $\Psi_j(r)$ are considered since the refractive index profile is radially symmetric, i.e. $n(x, y) = n(r)$. The above eigenvalue problem then becomes:

$$\frac{d^2\Psi_j}{dr^2} + \frac{1}{r}\frac{d\Psi_j}{dr} + \left(k^2 n^2(r) - \Lambda_j^2\right) \Psi_j = 0. \tag{2}$$

Normalization of the eigenfunctions can be achieved by requiring the inner product condition

$$\langle \Psi_i, \Psi_j \rangle = 2\pi \int_0^\infty \Psi_i \Psi_j^* r \mathrm{d}r = 2\pi \delta_{ij}, \tag{3}$$

where * denotes complex conjugation and $\delta_{ij}$ is the Kronecker delta. The brackets denote the standard inner-product notation. The mode fields $\Psi_j$ and the propagation constants $\Lambda_j$ can be determined numerically from Eq. (2) for a given function $n(r)$. Since the entire cavity is treated as one MMF, one can calculate $\Psi_j$ and $\Lambda_j$ using the design specifications of the MMF only. To be consistent with experiment, we assume the numerical aperture (NA) of the MMF to be 0.07, which is related to the core index $n_1$ and cladding index $n_2$ through the relationship $\mathrm{NA}^2 = n_1^2 - n_2^2$. For silica fibers, we assume $n_1 = 1.5008$ and $n_2 = 1.4992$ which gives a bulk index of $n = 1.5$. With a core radius of 10μm, the index profile in the cavity is then:

$$n(r) = \begin{cases} n_1 = 1.5008, & r \le 10\mu m \\ n_2 = 1.4992, & r > 10\mu m. \end{cases} \tag{4}$$

Fig. 2 shows the solutions to the eigenvalue problem (2), with wavelength $\lambda = 1.03\mu m$. For the parameters considered only two radially-symmetric modes are found ($LP_{01}$ and $LP_{02}$). These numerically found modes are consistent with the optical fiber specifications. Although coupling can occur between the $LP_{01}$ mode and any of the $LP_{11}$, $LP_{21}$ or $LP_{02}$ modes, a two-mode model is sufficient to characterize the essential multi-mode dynamics observed from simulations and experiments.

## B. Envelope Equations

The averaged intra-cavity propagation for the two modes $q_{1,2}(z, t)$ of the electric field envelope corresponding to the transverse mode fields $\Psi_{1,2}(x, y)$ can be represented by a system of coupled Ginzburg-Landau equations (CGLEs) in dimensionless form [44]:

$$i\frac{\partial q_1}{\partial z} + \frac{D}{2}\frac{\partial^2 q_1}{\partial t^2} + \left(\gamma_{11}|q_1|^2 + \gamma_{12}|q_2|^2\right) q_1 + C q_2 = iR_1, \tag{5}$$

$$i\left(\frac{\partial q_2}{\partial z}+s_2\frac{\partial q_2}{\partial t}\right)+\frac{D}{2}\frac{\partial^2 q_2}{\partial t^2}+\left(\gamma_{12}|q_1|^2+\gamma_{22}|q_2|^2\right)q_2+Cq_1=iR_2, \tag{6}$$

with $R_j$ ($j$ = 1, 2) given by:

$$R_j=\left[G_j(z)\left(1+\tau\partial_t^2\right)-\delta_j+\beta_j|q_j|^2-\mu_j|q_j|^4\right]q_j, \tag{7}$$

and the non-local function $G_j$ ($z$) is:

$$G_j(z)=\frac{2g_j}{1+\int_{-\infty}^{\infty}(|q_1|^2+|q_2|^2)\,dt}. \tag{8}$$

In the above formalism, $z$ is the propagation distance divided by the total cavity length, and $t$ is the retarded time normalized by the typical full-width at half-maximum of mode-locked pulses, i.e. 200fs. The parameter $D$ denotes the normalized group-velocity-dispersion (GVD), and is negative (positive) for normal (anomalous) dispersion. The effective self- and cross-phase modulations $\gamma_{ij}$ depend on the overlap-integrals between the transverse modal structures as well as the setting of the saturable absorber. Strictly speaking the saturable absorber can produce effective quintic modifications to the nonlinear index, but numerical simulations show that they do not affect the pulse dynamics significantly and hence are neglected in the present model. The linear coupling term $C$ describes the interchange of energy between the modes which arises from fluctuations of refractive index in the propagating direction as well as microbending of the fiber core.

The dissipative effects are captured in expressions (6) and (7). Here $G_j$ ($z$) represents the gain with pumping strength $2g_j$ experienced by the $j^{th}$ mode, and it is saturated by the total cavity energy given by the integral in the denominator. The bandwidth of the gain is denoted by the parameter $\tau$. $\beta_j$ and $\mu_j$ are positive quantities that model the distributed effective saturable absorption in the cavity. The cross-saturations between the modes have been neglected since they don't have significant impact on the dynamics. In the simulations that follow it is assumed that $\tau$, $\beta_j$ and $\mu_j$ are small. In practice, it is hard to change $g_1$ and $g_2$ independently. Roughly speaking, both fiber modes $q_{1,2}$ compete to saturate the same population inversion. More precisely, they have different spatial profiles $\Psi_{1,2}$ and spatially deplete the gain in a different way. This is a very complicated effect that requires using a spatial gain profile across the fiber [21], and will not be considered here. For simplicity we will assume a fixed ratio between the gain parameters $g_1$ and $g_2$.

The specific coupled fiber modes chosen in what follows are the $LP_{01}$ and $LP_{02}$ radially symmetric modes. The specific modes chosen are largely irrelevant as their overlap integrals calculated for use in the coefficients of the nonlinearities in Eq. (5) are only slightly modified. What is of primary importance is the linear coupling coefficient $C$ and the induced loss $\delta_2$, which we use here as independent variables to study their effects on mode-locking performance. Simulations performed of the mode-locked laser cavity using other coupled modes should show little essential change from those presented here.

## III. NUMERICAL SIMULATIONS

The numerical procedure employed for solving the CGLEs (5) uses a fourth-order Runge-Kutta method in $z$ and spectral (Fourier) transforms in the time variable $t$. Fig. 3 shows the

ideal mode-locking behavior starting from white-noise. Stable mode-locked pulses are formed after approximately a hundred round-trips of the laser cavity. The same mode-locked state is achieved regardless of the initial condition used, thus confirming that the solution is a global attractor and the mode-locking process is self-starting.

It is well known that multi-pulsing can occur in single-mode fiber lasers when too much energy is injected into the cavity. This kind of multi-pulsing instability is also observed for the MMF laser considered in this paper. Fig. 4 shows the mechanism for which a single pulse splits into two or more pulses when the pumping strength is increased. For the parameters used in Fig. 4, stable single-pulse mode-locking can be achieved up to $g_1 = 4.4$. When the pumping strength exceeds this value, the pulse starts to shred energy in the form of radiation, which is the first step towards multi-pulsing instability. At higher values of $g_1$ a periodic solution is formed. This periodic solution consists of two peaks that undergo tunneling indefinitely, i.e. one peak reaches its maximum when the other one reaches the minimum. When the gain is large enough, such periodic solution is unstable. In this case the initial condition quickly evolves into two identical pulses with constant separation. Three or more pulses can be achieved by ramping up $g_1$.

It is useful to study how the second mode content affects the multi-pulsing instability. In the simulations, there are three ways to change the amount of second mode $q_2$ circulating in the cavity. The first way is to change the ratio between $g_1$ and $g_2$, i.e. varying $a = g_1/g_2$. The gain received by the second mode can be increased by decreasing $a$. In practice, however, this method may be difficult to perform since the relationship between $g_1$ and $g_2$ is fixed once the spatial profile of the dopant is determined [21]. Adjusting $a$ may require changing the doping material, and therefore this will not be further investigated in this paper. The second way to control the second mode content is to adjust the linear coupling $C$ between the modes, which controls the energy transfer between $q_1$ and $q_2$ in the cavity. The third way to change the second mode content is to control the higher-order mode loss parameter $\delta_2$. Experimentally this can be done by coiling the gain fiber as shown in Fig. 1 [20]. A smaller diameter induces a larger suppression to the higher modes in the cavity while the fundamental mode $q_1$ is almost unaffected above a certain radius. Strictly speaking, changing the coiling diameter may modify the linear coupling $C$ between the modes. In this paper we assume their correlation is weak so that $\delta_2$ and $C$ can be tuned independently.

The first column of Fig. 5 shows the performance of the MMF laser as a function of the linear coupling $C$. The total cavity energy, which is defined as

$$E = \int_{-\infty}^{\infty} \left( |q_1|^2 + |q_2|^2 \right) \mathrm{d}t, \tag{9}$$

is recorded right before multi-pulsing instability occurs. In general, a larger linear coupling promotes the energy transfer from the fundamental mode to the second mode (and other higher modes if they exist) and hence allowing for a higher second mode content in the cavity. In the extreme case where linear coupling between the modes is absent, i.e. $C = 0$, the second mode locks into the zero solution and the energy ($E = 6.8998$) is the smallest among all the recorded values. When $C$ is nonzero, $q_2$ contributes to −34 dB of the total cavity energy at $C = 0.05$, and around −16 dB at $C = 0.45$ (see bottom left of Fig. 5). Meanwhile the maximum total cavity energy before multi-pulsing first increases from $E = 6.97$ to a maximum of $E = 7.733$ at $C = 0.3$, and then decreases again to $E = 7.52$ at $C = 0.45$. In other words, in the region $0.05 \leq C \leq 0.3$, adding more second mode content to the cavity actually improves the performance of the laser as higher pulse energy can be achieved. In contrary, further increasing the linear coupling beyond the value $C = 0.3$

destabilizes the mode-locking operation and hinders the maximum pulse energy obtained. This corresponds to an MPI of ~−20 dB, within the same order of magnitude as the experimental threshold for reduced single pulse energies.

The performance of the laser as a function of the second mode loss $\delta_2$ is shown in the second column of Fig. 5. The pulse energy increases monotonically from $E = 7.4$ at $\delta_2 = 1.2$ to $E = 8.1013$ at $\delta_2 = 1.8$. Further suppressing the second mode ($\delta_2 > 1.8$) results in a drop of pulse energy. In the limiting case where $\delta_2 \to \infty$, the second mode content in the cavity is so small that the single-mode approximation becomes valid. In this situation the pulse energy approaches $E = 6.8998$, which is the same as that obtained by setting $C = 0$. On the other hand, it maybe difficult or even impossible to achieve mode-locking if the second mode suppression is not enough. Fig. 6 shows the small mode-locked region when $\delta_2 = 1.2$. Specifically, stable single pulse mode-locking is only possible in a small window in the range $4.79 < g_1 < 4.81$. We were not able to find other operating regimes for stable single pulse mode-locking outside this region. The range of $g_1$ values for which stable single-pulse mode-locking can occur is shown in Fig. 7. One can see that the operating regime is extended when the suppression of $q_2$ increases. The window of admissible $g_1$ values is largest in the limiting case where $q_2$ is completely removed from the cavity, ranging from $g_1 = 3.9$ to below 1.5. A similar trend is also observed when the linear coupling $C$ is varied. In general, the window of single-pulse operating regime is the largest when $C = 0$, and the width of the window decreases monotonically with increasing $C$. These observations indicate that excessive amounts of the second mode can have deleterious effects on the stability of mode-locking dynamics, confirming the experimental observation of lower maximum single pulse energies in LMA fiber lasers propagating multiple modes.

## IV. EXPERIMENTAL FINDINGS

The experimental behavior of mode-locked lasers based on multimode fibers will now be studied. Different fiber designs and mode control mechanisms will be considered.

The most straightforward way to scale to larger fiber cores is by using large mode-area step-index MMF while attempting to strip off higher-order modes. We built the ANDi cavity presented in Fig. 8. The gain medium is about 1.2 m of Yb-doped double-clad fiber with a core diameter of 20 μm (Liekki Yb1200-20/125). The 125 μm cladding diameter offers simple integration to telecommunication grade fiber components. The numerical aperture (NA) is 0.07, yielding a mode-field diameter (MFD) of 17 μm and a V-number of 4.3, supporting four waveguide modes. By solving the waveguide eigenvalue problem [19], the HOM closest to the fundamental $LP_{01}$ mode is found to be $LP_{11}$, with a group-velocity mismatch (GVM) of 0.80 ps/m. Light from a 975 nm pump diode is injected into the cladding of the gain fiber using a homemade side-fused pump-signal combiner. To favor fundamental mode excitation, the combination of 0.35 m of fiber with an 8 μm core diameter and 0.14 NA and 0.45 m of 10 μm core diameter single-mode fiber (SMF) with a NA of 0.08 are spliced to the gain fiber through a tapered mode-field adapter inside the combiner. The total cavity length is brought to 2.6 m by splicing 0.6 m of matching passive 20 μm multimode fiber after the gain fiber. A cladding mode stripper after the gain fiber removes residual pump light. Nonlinear polarization rotation in the fibers is converted to self-amplitude modulation by three waveplates and a polarizing beamsplitter. This NPE port also serves as the output coupler. A polarizing isolator ensures unidirectional ring operation. A quartz plate placed before the isolator creates a birefringent spectral filter, enabling dissipative soliton pulse shaping. Two perpendicular coils in the gain fiber provide high loss to the higher order modes with little loss to the fundamental mode [20]. An external grating pair acts as a dispersive delay line to compensate the chirp of the output pulses.

We first operate the laser without coiling the gain fiber and thus without higher-order mode filtering. After tuning the NPE waveplates, the laser provides a stable, self-starting mode-locked pulse train at a repetition rate of 77 MHz. The mode-locked spectrum and dechirped interferometric autocorrelation (AC) using a 15-nm filter are presented in Fig. 9(a) and (b). The single-pulse energy is 4.4 nJ, and the full-width at half-maximum (FWHM) of the AC is 250 fs, giving a pulse duration of 177 fs using a gaussian deconvolution factor. Two smaller pulses are visible ~1.5 ps away from the main pulse. This agrees with a calculated intermodal delay of 1.4 ps between $LP_{01}$ and $LP_{11}$. The spectrum shows strong modulations with a few nm period due to multi-path interference (MPI). The Fourier transform of the spectrum shown in Fig. 9(c) qualitatively confirms the fringes correspond to the $LP_{11}$ intermodal delay. A quantitative assessment of the HOM content would require a spatially resolved measurement such as the $S^2$ method [51]. The $M^2$ parameter was measured to be 1.33, confirming the multimode nature of the beam. If the pump power is raised further, the mode-locked state becomes unstable, then locks into similar double- and triple-pulsing states as shown in Fig. 9(d). In the multi-pulsing states, the energy of each individual pulse is always nearly 4.2 nJ.

The linear coupling between fiber modes is determined by random refractive index variations and microbends in the fiber core, and can only be addressed during fiber fabrication. We instead control the higher order mode loss by coiling the fiber on two perpendicular axes [20]. We found mode-locked states with coiling diameters from 8 cm to 4 cm, with prohibitive bending losses at smaller diameters. Fig. 10(a) and (b) shows a single-pulsing mode-locked state at a coiling diameter of 4 cm with a 15 nm filter. The pulse energy is 21 nJ, and from the dechirped AC we infer a dechirped pulse duration of 115 fs. Filtering of the higher-order modes clearly allows higher pulse energies. This wide-bandwidth mode is similar to the highly structured mode in Fig. 12(h) of [13]. Up to its sensitivity limit, the autocorrelation trace shows no secondary pulse at the $LP_{11}$ delay, confirming lower HOM content. Fig. 10(c) and (d) present a similarly stabilized mode-locked state with a coiling diameter of 4 cm and a 20 nm filter. The pulse energy and inferred dechirped duration are 12 nJ and 150 fs. Secondary $LP_{11}$ pulses are again not detected above the noise floor of the autocorrelation.

Although energies of up to 21 nJ are achieved in this multimode step-index fiber cavity, this performance is well below that of a previously-built laser with 10 μm core diameter single-mode fiber [52]. This laser provided pulse energies up to 31 nJ with a similar 2 m cavity. By scaling the MFD from 11 μm to 17 μm, we would expect pulse energies up to 75 nJ from the 20 μm core ANDi. This indicates that despite coiling, higher-order modes are not sufficiently controlled in the step-index LMA cavity, and their presence limits the maximum single pulsing energy that can be stabilized.

An optimal mode control mechanism should be built into the fiber design rather than depend on external manipulations. One such mechanism is the large mode-area photonic crystal fiber. We present results from a laser built around such a LMA PCF. The details of the setup as well as representative mode-locked states are discussed elsewhere [17]. The central element is 1.25 m of Yb-doped LMA PCF with a core diameter of 40 μm, an effective NA of 0.03 and a MFD of ~33 μm. The photonic lattice is hexagonal with a pitch of 12.3 μm and a hole diameter of 1.1 μm [53]. Although this seven missing hole design is not endlessly single mode, the modal propagation constants are far enough to suppress intermodal coupling over the length of the fiber. This results in effectively single-mode behavior if the fundamental mode is properly seeded.

Two lasers were built using the same cavity design and distinct PCFs with essentially identical specifications (Crystal Fibre DC-170-40-Yb and DC-170-40-Yb-2). Fig. 11 shows

self-starting mode-locked states obtained using each fiber. The first fiber is presented in Fig. 11(a)–(b) and yields a single pulsing state with energy 124 nJ, and the state from the second fiber in Fig. 11(c)–(d) is double pulsing with an average energy of 47 nJ per pulse. The first PCF laser shows very weak spectral modulations and no visible secondary pulse on its autocorrelation, indicating essentially singlemode propagation. Although the fibers are essentially singlemode by specification, the second fiber clearly displays significant higher-order mode content as evidenced by the strong modulations on the mode-locked spectrum. This could be due to inconsistencies in the fabrication process allowing higher-order modes to be guided. Excitation of multiple modes at the fiber input could also seed secondary modes, although identical setups and alignment procedures were used for both lasers. The singlemode PCF yields single pulse energies of up to 154 nJ, limited by available pump power, while the effectively multimode PCF only provides up to 60 nJ before the onset of multipulsing instabilities. This corroborates the conclusions from the step-index ANDi laser that the presence of unfiltered higher-order mode content limits the maximum single pulse energy accessible in the cavity.

Another distributed and built-in mode filtering mechanism is provided by chiraly-coupled core (CCC) fibers [22]. In such a fiber, a secondary core is wrapped in a helix around the main core. The pitch and chirality of the helix are chosen to selectively couple out modes other than the fundamental through quasi-phasematched resonances.We show results from an ANDi laser based on 3.9 m of Yb-doped CCC fiber. The fiber core diameter is 33.5 μm with a NA of 0.06. This yields a MFD of 21 μm and V = 6.03, supporting six modes. The $LP_{11}$ mode has a calculated GVM of 0.5 ps/m with $LP_{01}$. A detailed characterization of the performance of the laser is presented elsewhere [54]. Here we put the results in the context of multimode propagation. Fig. 12 presents a self-starting single-pulsing state obtained with an 8 nm filter. The pulse energy is 47 nJ and we infer a dechirped pulse duration of 225 fs from the AC. The small spectral modulation at the center indicate low HOM content, confirmed by the absence of any secondary pulse up to the 30 dB noise floor of the autocorrelation trace. The $M^2$ is measured to be 1.1 to 1.15 in CW and mode-locked states, confirming HOM filtering. When normalized to the mode-area of the fiber, these results are comparable to those a single-mode ANDi laser with similar dispersion and output spectral bandwidth. Pulse energies of about 4–5 nJ and 200 fs dechirped durations are shown in Fig. 12(f) and Fig. 13 of [13], using a fiber with a mode area 12 times smaller. This confirms that the robust and continuous mode filtering in the CCC fiber helps stabilize a multimode core to singlemode mode-locked performance.

The presented experimental findings clearly indicate that unsuppressed higher-order spatial modes severely affect the performance of mode-locked fiber lasers. Whereas HOM content in amplifiers and CW lasers mainly affects beam quality, the experiments presented here show that the maximum stable single pulse energy achievable in mode-locked oscillators is greatly reduced from the limit expected by scaling the core size. This is consistent with the numerical simulations above, which indicate that mode-locking is fundamentally destabilized when secondary mode content becomes significant enough. Experimentally, large core step-index fiber shows the largest performance degradation, yielding about 4 nJ of pulse energy compared to an expected energy of 75 nJ. Mode-filtering using selective bend loss raises the maximum pulse energy to 20 nJ, but still underperforms singlemode sources. In practice, full pulse energy scaling is achievable only with careful mode management mechanisms. This is demonstrated for large mode-area PCF as well as chirally-coupled core fibers whose mode-locked performance scales as expected with core size. It should be noted that PCFs with core diameters larger than 40 μm require the addition of extra mode filtering in the cavity. Indeed, photonic crystal rod lasers, such as in [15], [16], use a piece of single mode fiber as an intracavity spatial mode filter.

## V. CONCLUSION

The influence of multiple transverse modes on a mode-locked large mode area fiber laser cavity has been investigated both theoretically and experimentally. The motivation for using large core multi-mode fiber is to reduce the non-linear phase-shift for a given peak power in the mode-locked cavity. Excessive non-linear phase induces multi-pulsing instabilities in the laser cavity, thus limiting the total energy delivered in a single pulse. This multi-pulsing instability presents a fundamental limit that must be avoided in order to increase the performance of mode-locked lasers. We compared the performance of lasers based on coiled 20 μm core diameter step-index fiber, 40 μm core endlessly single-mode photonic crystal fiber and 33 μm core chirally-coupled core fiber.

Although the peak intensities are indeed reduced, the higher-order mode content that results from mode-coupling induces multi-pulsing instabilities. These prevent the scaling to higher peak powers with mode area. A detailed theoretical model, the first to characterize multi-mode laser mode-locking, is developed and shows that mode-locking is destabilized by excessive higher-order mode content. This results in a narrower range of stable single-pulse solutions and reduced maximum pulse energy when compared to single-mode fibers, consistent with the experimental findings. This model provides a framework to optimize the performance of the multi-mode fiber laser as a function of the various cavity parameters such as the suppression of higher-order mode content and coupling between modes. Experimentally, cavities with excessive higher-order mode content were found to have lowered normalized single pulse energies than equivalent single-mode lasers, consistent with the multi-pulsing instabilities observed in the numerical model. This is a much stronger drawback than in amplifiers or continuous-wave lasers, where multiple modes mainly affect beam quality. Selective bend loss in a step-index fiber is found to be insufficient to attain full single-mode performance. The expected pulse energies are achieved with fibers incorporating continuous mode filtering in their design, such as effectively single-mode PCF and chirally-coupled core fibers. Our findings confirm that, due to presence of higher-order mode content, large mode area fiber lasers must be carefully engineered to continuously suppress higher-order modes in order for their performance to surpass that of standard single-mode fiber lasers.

## Acknowledgments

The authors would like to acknowledge insightful conversations about multi-mode mode-locking performance with K. Kieu, W. Renninger, Y. Deng, and J. D. Kafka.

The work at Cornell was supported in part by the National Science Foundation (NSF) under Grant ECCS 0901323 and the National Institutes of Health under Grant EB002019. The work of J. N. Kutz was supported in part by the NSF under Grant DMS-0604700 and Grant DMS-1007621 and the Air Force Office of Scientific Research under Grant FA9550-09-0147. The work of S. Lefrancois was supported in part by the Fond Québécois de Recherche sur la Nature et les Technologies.

## REFERENCES

1. Haus HA. Mode-locking of lasers. IEEE J. Sel. Topics Quantum Electron. 2000 Nov.–Dec.; vol. 6(no. 6):1173–1185.
2. Wise FW, Chong A, Renninger WH. High-energy femtosecond fiber lasers based on pulse propagation at normal dispersion. Laser & Photon. Rev. 2008 Apr.; vol. 2(nos. 1–2):58–73.
3. Kutz JN. Mode-locked soliton lasers. SIAM Rev. 2006 Nov.; vol. 48(no. 4):629–678.
4. Namiki S, Ippen EP, Haus HA, Yu CX. Energy rate equations for mode-locked lasers. J. Opt. Soc. Amer. B. 1997; vol. 14(no. 8):2099–2111.

5. Soto-Crespo JM, Grapinet M, Grelu P, Akhmediev N. Bifurcations and multiple-period soliton pulsations in a passively mode-locked fiber laser. Phys. Rev. E. 2004 Dec.; vol. 70(no. 6): 066612-1–066612-11.
6. Kutz JN, Sandstede B. Theory of passive harmonic mode-locking using waveguide arrays. Opt. Exp. 2008; vol. 16(no. 2):636–650.
7. Mollenauer, LF.; Gordon, JP. Solitons in Optical Fibers: Fundamentals and Applications. New York: Academic; 2006.
8. Tamura K, Ippen EP, Haus HA, Nelson LE. 77-fs pulse generation from a stretched-pulse mode-locked all-fiber ring laser. Opt. Lett. 1993; vol. 18(no. 13):1080–1082. [PubMed: 19823296]
9. Buckley JR, Wise FW, Ilday FÖ, Sosnowski T. Femtosecond fiber lasers with pulse energies above 10 nJ. Opt. Lett. 2005; vol. 30(no. 14):1888–1890. [PubMed: 16092379]
10. Ilday FÖ, Wise FW, Sosnowski T. High-energy femtosecond stretched-pulse fiber laser with a nonlinear optical loop mirror. Opt. Lett. 2002; vol. 27(no. 17):1531–1533. [PubMed: 18026496]
11. Ilday FO, Buckley JR, Clark WG, Wise FW. Self-similar evolution of parabolic pulses in a laser. Phys. Rev. Lett. 2004 May; vol. 92(no. 21):213902-1–213902-4. [PubMed: 15245282]
12. Chong A, Buckley J, Renninger W, Wise F. All-normal-dispersion femtosecond fiber laser. Opt. Exp. 2006; vol. 14(no. 21):10095–10100.
13. Chong A, Renninger WH, Wise FW. Properties of normal-dispersion femtosecond fiber lasers. J. Opt. Soc. Amer. B. 2008; vol. 25(no. 2):140–148.
14. Renninger WH, Chong A, Wise FW. Dissipative solitons in normal-dispersion fiber lasers. Phys. Rev. A. 2008 Feb.; vol. 77(no. 2):023814-1–023814-4.
15. Ortaç B, Baumgartl M, Limpert J, Tünnermann A. Approaching microjoule-level pulse energy with mode-locked femtosecond fiber lasers. Opt. Lett. 2009; vol. 34(no. 10):1585–1587.
16. Lecaplain C, Ortaç B, Machinet G, Boullet J, Baumgartl M, Schreiber T, Cormier E, Hideur A. High-energy femtosecond photonic crystal fiber laser. Opt. Lett. 2010; vol. 35(no. 19):3156–3158. [PubMed: 20890318]
17. Lefrancois S, Kieu K, Deng Y, Kafka JD, Wise FW. Scaling of dissipative soliton fiber lasers to megawatt peak powers by use of large-area photonic crystal fiber. Opt. Lett. 2010; vol. 35(no. 10): 1569–1571. [PubMed: 20479811]
18. Renninger WH, Chong A, Wise FW. Area theorem and energy quantization for dissipative optical solitons. J. Opt. Soc. Amer. B. 2010; vol. 27(no. 10):1978–1982.
19. Marcuse, D. Theory of Dielectric Optical Waveguides. New York: Academic; 1974.
20. Koplow JP, Kliner DAV, Goldberg L. Single-mode operation of a coiled multimode fiber amplifier. Opt. Lett. 2000 Apr.; vol. 25(no. 7):442–444. [PubMed: 18064073]
21. Marciante JR. Gain filtering for single-spatial-mode operation of large-mode-area fiber amplifiers. IEEE J. Sel. Topics Quantum Electron. 2009 Jan.; vol. 15(no. 1):30–36.
22. Liu, C-H.; Chang, G.; Litchinitser, N.; Galvanauskas, A.; Guertin, D.; Jacobson, N.; Tankala, K. Proc. Adv. Solid State Photon. Vancouver, BC, Canada: 2007 Jan.. Effectively single-mode chirally-coupled core fiber. no. ME2
23. Fermann M, Galvanauskas A, Hofer M. Ultrafast pulse sources based on multi-mode optical fibers. Appl. Phys. B. 2000; vol. 70(no. 7):13–23.
24. Tamura K, Haus HA, Ippen EP. Self-starting additive pulse mode-locked erbium fibre ring laser. Electron. Lett. 1992 Nov.; vol. 28(no. 24):2226–2228.
25. Haus HA, Ippen EP, Tamura K. Additive-pulse mode-locking in fiber lasers. IEEE J. Quantum Electron. 1994 Jan.; vol. 30(no. 1):200–208.
26. Leblond H, Salhi M, Hideur A, Chartier T, Brunel M, Sanchez F. Experimental and theoretical study of the passively mode-locked ytterbium-doped double-clad fiber lasers. Phys. Rev. A. 2002 Jun.; vol. 65(no. 6):063811-1–063811-9.
27. Brabec T, Spielmann C, Curley PF, Krausz F. Kerr lens mode locking. Opt. Lett. 1992; vol. 17(no. 18):1292–1294. [PubMed: 19798161]
28. Spinelli, L.; Couilland, B.; Goldblatt, N.; Negus, DK. Proc. Conf. Lasers Electro-Opt. OSA Tech. Dig. Ser. Vol. vol. 10. Washington D.C.: 1991. no. CPDP7

29. Duling IN III. Subpicosecond all-fibre erbium laser. Electron. Lett. 1991 Mar.; vol. 27(no. 6):544–545.
30. Richardson DJ, Laming RI, Payne DN, Matsas VJ, Phillips MW. Selfstarting, passively modelocked erbium fibre ring laser based on the amplifying Sagnac switch. Electron. Lett. 1991 Mar.; vol. 27(no. 6):542–544.
31. Dennis ML, Duling IN III. High repetition rate figure eight laser with extracavity feedback. Electron. Lett. 1992 Sep.; vol. 28(no. 20):1894–1896.
32. Ilday FÖ, Wise FW, Sosnowski T. High-energy femtosecond stretched-pulse fiber laser with a nonlinear optical loop mirror. Opt. Lett. 2002; vol. 27(no. 17):1531–1533. [PubMed: 18026496]
33. Kärtner FX, Kopf D, Keller U. Solitary-pulse stabilization and shortening in actively mode-locked lasers. J. Opt. Soc. Amer. B. 1995; vol. 12(no. 3):486–496.
34. Haus H. A theory of forced mode locking. IEEE J. Quantum Electron. 1975 Jul.; vol. 11(no. 7): 323–330.
35. Kutz, JN. Mode-locking of fiber lasers via nonlinear mode-coupling. In: Akhmediev, NN.; Ankiewicz, A., editors. Dissipative Solitons (Lecture Notes in Physics). Berlin, Germany: Springer-Verlag; 2005. p. 241-265.
36. Proctor JL, Kutz JN. Passive mode-locking by use of waveguide arrays. Opt. Lett. 2005; vol. 30(no. 15):2013–2015. [PubMed: 16092250]
37. Proctor J, Kutz JN. Nonlinear mode-coupling for passive mode-locking: Applications of waveguide arrays, dual-core fibers, and/or fiber arrays. Opt. Exp. 2005; vol. 13(no. 22):8933–8950.
38. Intrachat K, Kutz JN. Theory and simulation of passive mode-locking dynamics using a long-period fiber grating. IEEE J. Quantum Electron. 2003 Dec.; vol. 39(no. 12):1572–1578.
39. Renninger WH, Chong A, Wise FW. Dissipative solitons in normal-dispersion fiber lasers. Phys. Rev. A. 2008 Feb.; vol. 77(no. 2):023814-1–023814-4.
40. Soto-Crespo JM, Akhmediev NN, Afanasjev VV, Wabnitz S. Pulse solutions of the cubic-quintic complex Ginzburg-Landau equation in the case of normal dispersion. Phys. Rev. E. 1997 Apr.; vol. 55(no. 4):4783–4796.
41. Komarov A, Leblond H, Sanchez F. Multistability and hysteresis phenomena in passively mode-locked fiber lasers. Phys. Rev. A. 2005 May; vol. 71(no. 5):053809-1–053809-9.
42. Komarov A, Leblond H, Sanchez F. Quintic complex Ginzburg-Landau model for ring fiber lasers. Phys. Rev. E. 2005 Aug.; vol. 72(no. 2):025604-1–025604-4.
43. Ding E, Kutz JN. Operating regimes, split-step modeling, and the Haus master mode-locking model. J. Opt. Soc. Amer. B. 2009; vol. 26(no. 12):2290–2300.
44. Kutz JN, Eggleton BJ, Stark JB, Slusher RE. Nonlinear pulse propagation in long-period fiber gratings: Theory and experiment. IEEE J. Sel. Topics Quantum Electron. 1997 Oct.; vol. 3(no. 5): 1232–1245.
45. Crosignani B, Di Porto P. Soliton propagation in multimode optical fibers. Opt. Lett. 1981; vol. 6(no. 7):329–330. [PubMed: 19701421]
46. Kolesik M, Moloney JV. Nonlinear optical pulse propagation simulation: From Maxwell's to unidirectional equations. Phys. Rev. E. 2004 Sep.; vol. 70(no. 3):036604-1–036604-11.
47. Chaipiboonwong T, Horak P, Mills JD, Brocklesby WS. Numerical study of nonlinear interactions in a multimode waveguide. Opt. Exp. 2007; vol. 15(no. 14):9040–9047.
48. Poletti F, Horak P. Description of ultrashort pulse propagation in multimode optical fibers. J. Opt. Soc. Amer. B. 2008; vol. 25(no. 10):1645–1654.
49. Kapitula T, Kutz JN, Sandstede B. Stability of pulses in the master mode-locking equation. J. Opt. Soc. Amer. B. 2002; vol. 19(no. 4):740–746.
50. Kapitula T, Kutz JN, Sandstede B. The Evans function for nonlocal equations. Ind. Univ. Math. J. 2004; vol. 53(no. 4):1095–1126.
51. Nicholson JW, Yablon AD, Ramachandran S, Ghalmi S. Spatially and spectrally resolved imaging of modal content in large-mode-area fibers. Opt. Exp. 2008; vol. 16(no. 10):7233–7243.
52. Kieu K, Renninger WH, Chong A, Wise FW. Sub-100 fs pulses at watt-level powers from a dissipative-soliton fiber laser. Opt. Lett. 2009; vol. 34(no. 5):593–595. [PubMed: 19252562]

53. Limpert J, Liem A, Reich M, Schreiber T, Nolte S, Zellmer H, Tünnermann A, Broeng J, Petersson A, Jakobsen C. Low-nonlinearity single-transverse-mode ytterbium-doped photonic crystal fiber amplifier. Opt. Exp. 2004; vol. 12(no. 7):1313–1319.

54. Lefrancois S, Sosnowski TS, Liu C-H, Galvanauskas A, Wise FW. Energy scaling of mode-locked fiber lasers with chirally-coupled core fiber. Opt. Exp. 2011; vol 19(no. 4):3464–3470.

## Biographies

**Edwin Ding** received the B.Eng. degree in mechanical engineering from the University of Hong Kong, Hong Kong, in 2006. He is currently pursuing the Ph.D. degree in the Department of Applied Mathematics, University of Washington, Seattle.

**Simon Lefrancois** received the B.Sc. degree in physics from Laval University, Quebec City, QC, Canada, in 2007. He is currently pursuing the Ph.D. degree in the Department of Applied Physics, Cornell University, Ithaca, NY.

**Jose Nathan Kutz** received the B.S. degree in physics and mathematics from the University of Washington, Seattle, in 1990, and the Ph.D. degree in applied mathematics from Northwestern University, Evanston, IL, in 1994.

He is currently a Professor and Chair of Applied Mathematics at the University of Washington.

**Frank W. Wise** received the B.S. degree from Princeton University, Princeton, NJ, the M.S. degree from the University of California, Berkeley, and the Ph.D. degree from Cornell University, Ithaca, NY.

He is currently a Professor and Chair of Applied Physics at Cornell University.

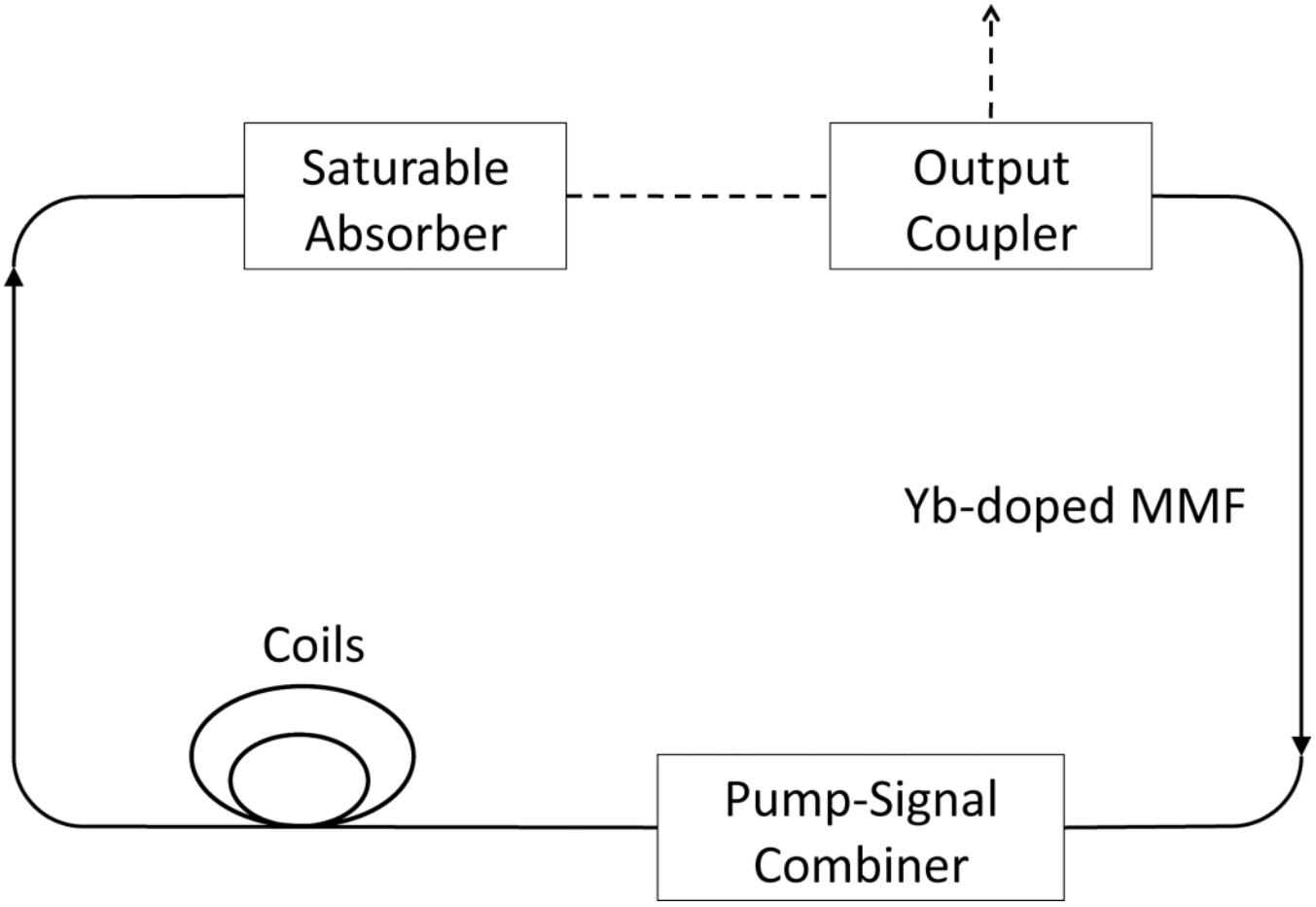


**Fig. 1.**
Idealized experimental setup based upon Fig. 8. The entire laser cavity is approximated by a single MMF.

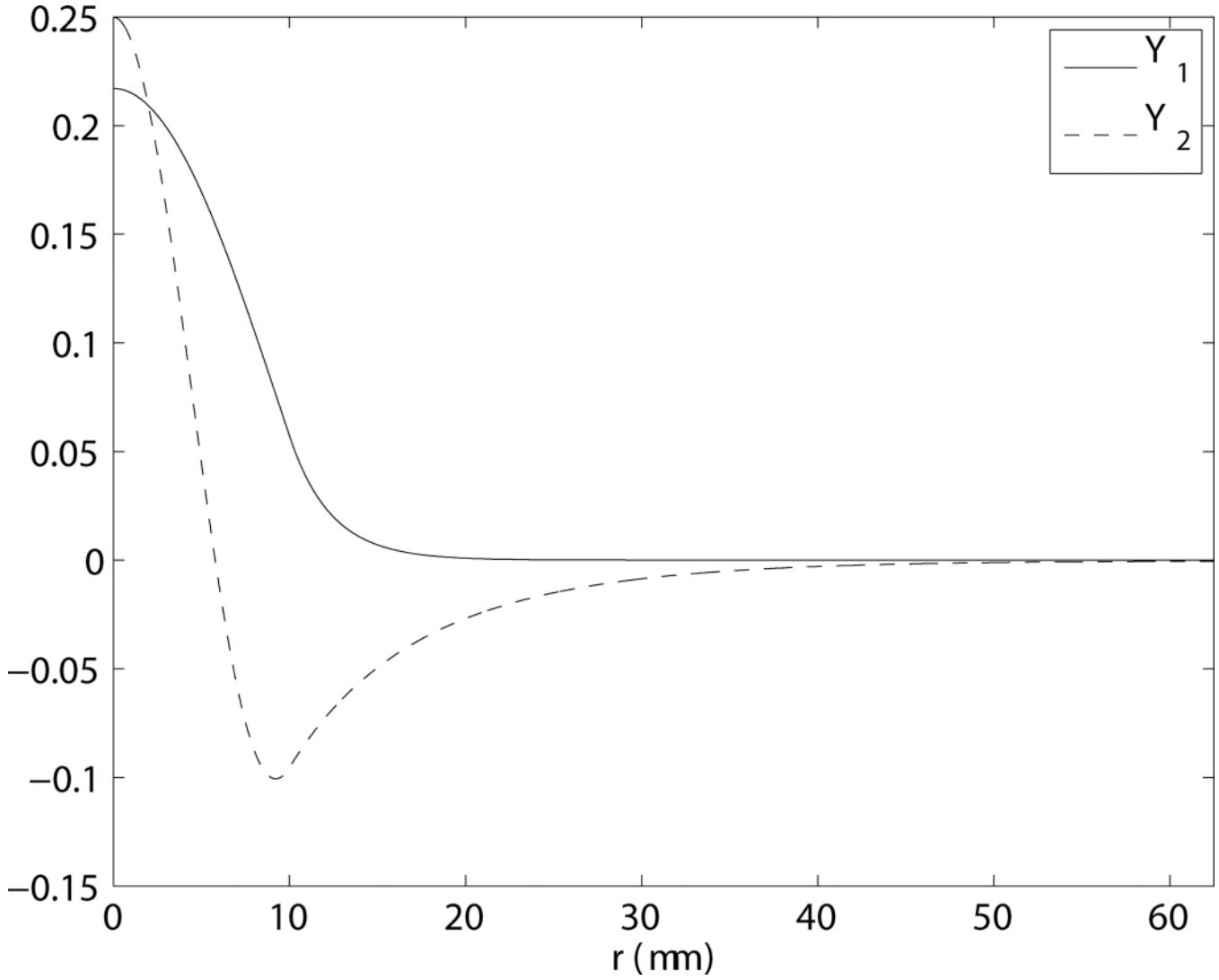


**Fig. 2.**
Radially symmetric mode fields for the eigenvalue problem (2). Here $n(r)$ is the index profile given by (4) and $k = 2\pi/\lambda$, where $\lambda = 1.03\mu m$ is the wavelength.

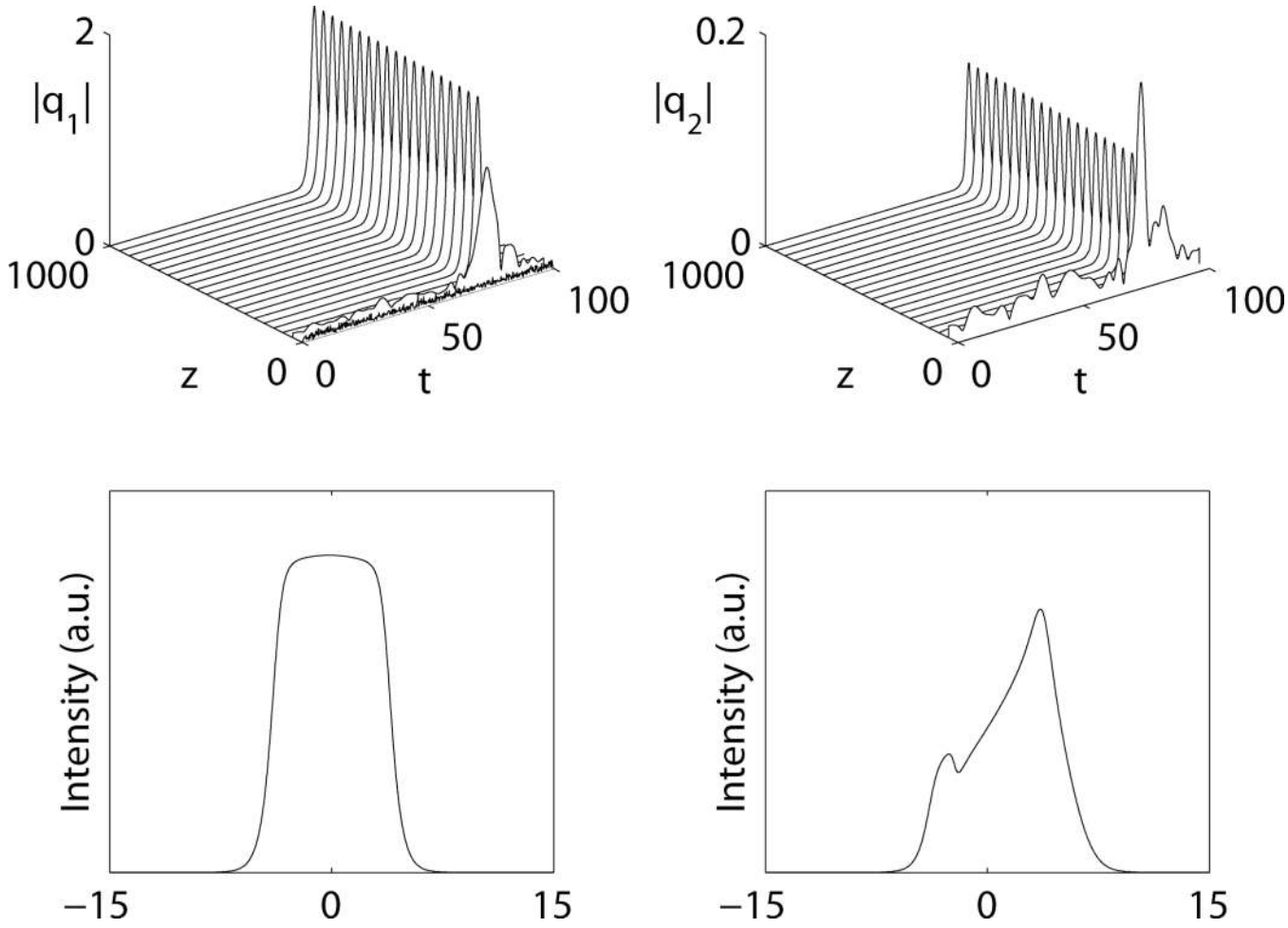


**Fig. 3.**

Top: Evolution of fiber modes from white-noise where the second mode $q_2$ is initially zero. Stable mode-locked state is achieved after about a hundred dispersion scales. The parameters used are $D = -0.4$, $s_2 = 1$, $(\gamma_{11}, \gamma_{22}, \gamma_{12}) = (1.2, 1.1, 2.3)$, $(\beta_1, \beta_2) = (0.3, 0.28)$, $(\mu_1, \mu_2) = (0.023, 0.022)$, $C = 0.15$, $(g_1, g_2) = (4, 3.077)$, $\tau = 0.1$, and $(\delta_1, \delta_2) = (1, 1.2)$. Bottom: The corresponding spectrum of the mode-locked state.

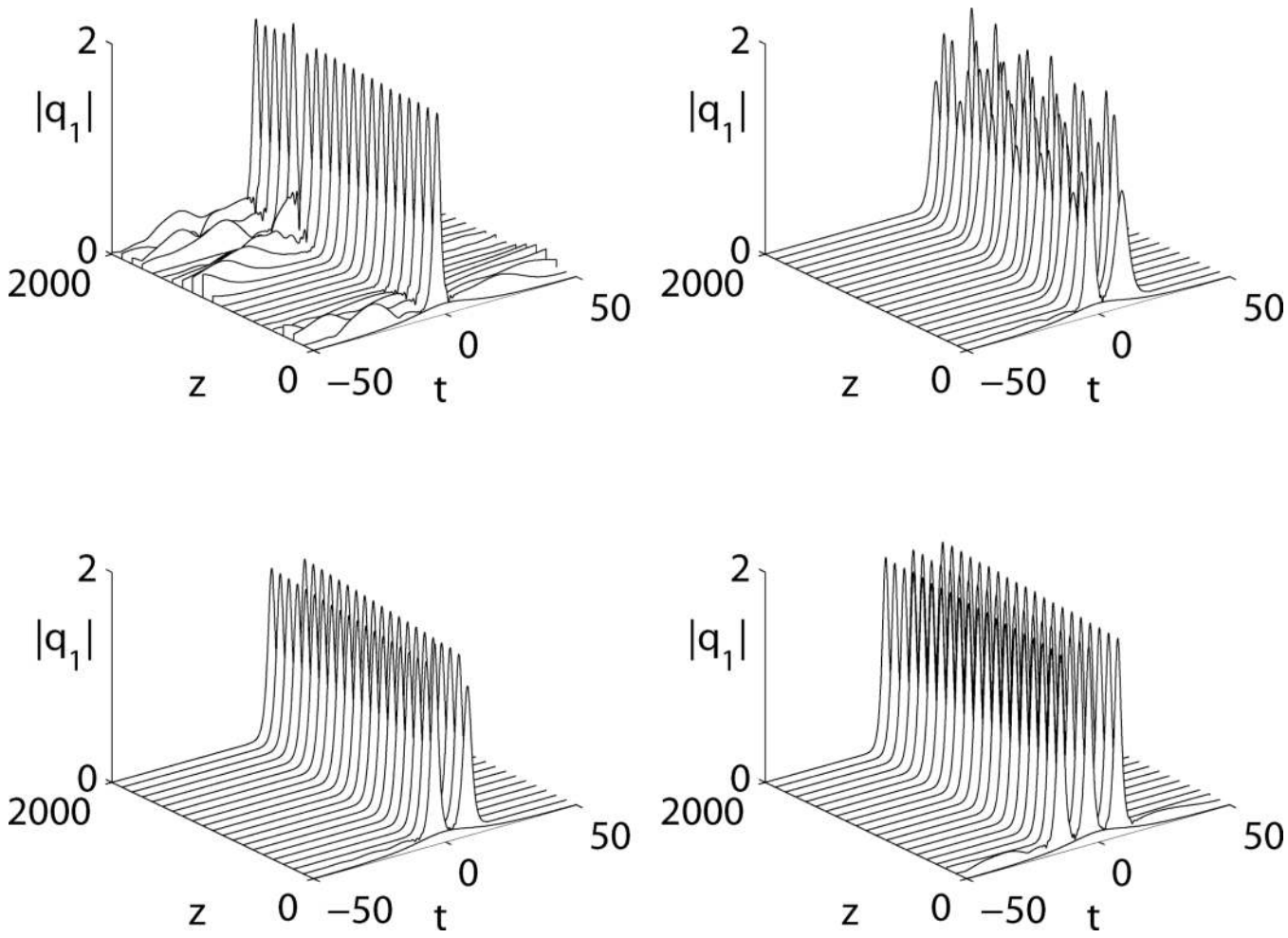


**Fig. 4.**

Top left: Shredding of energy at $g_1 = 5$, which is the onset of multi-pulsing instability. Top right: Periodic solution at $g_1 = 6.5$. Bottom left: Stable double-pulse solution at $g_1 = 7$. Bottom right: Stable triple-pulse solution at $g_1 = 12$. The rest of the parameters are $D = -0.4$, $s_2 = 1$, $(\gamma_{11}, \gamma_{22}, \gamma_{12}) = (1.2, 1.1, 2.3)$, $(\beta_1, \beta_2) = (0.3, 0.28)$, $(\mu_1, \mu_2) = (0.023, 0.022)$, $C = 0.15$, $g_2 = g_1/1.3$, $\tau = 0.1$, and $(\delta_1, \delta_2) = (1, 1.2)$.

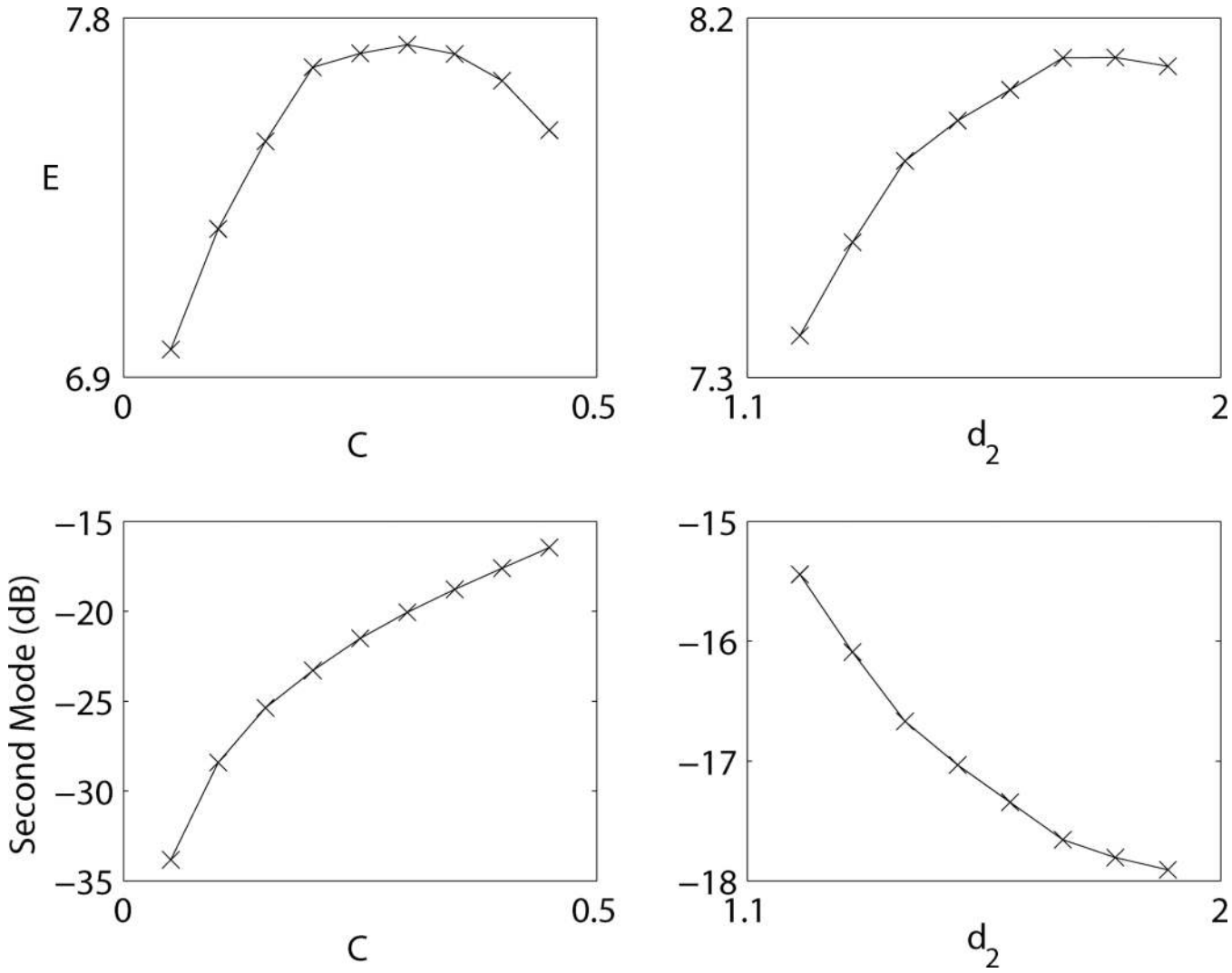


**Fig. 5.**

Top: Maximum total cavity energy obtained right before the onset of multi-pulsing instability as a function of different cavity parameters. Bottom: The corresponding second mode content in the cavity. Unless otherwise specified, the parameters used are $D = -0.4$, $s_2 = 1$, $(\gamma_{11}, \gamma_{22}, \gamma_{12}) = (1.2, 1.1, 2.3)$, $(\beta_1, \beta_2) = (0.3, 0.28)$, $(\mu_1, \mu_2) = (0.023, 0.022)$, $C = 0.5$, $g_1/g_2 = 1.3$, $\tau = 0.1$, and $(\delta_1, \delta_2) = (1, 1.2)$.

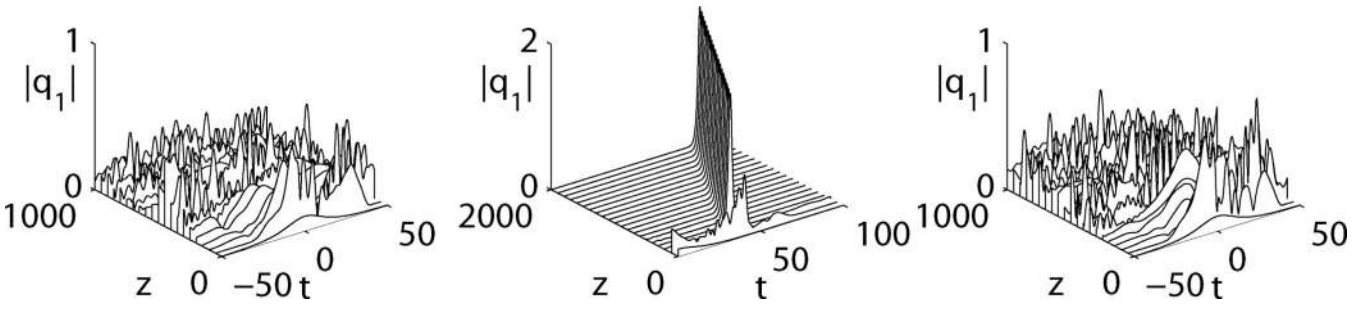


**Fig. 6.**

Small window of stable mode-locking when the suppression of the second mode is insufficient. Left: $g_1 = 4.79$. Middle: $g_1 = 4.8$. Right: $g_1 = 4.85$. $\delta_2 = 1.2$ and $C = 0.5$ for all the simulations.

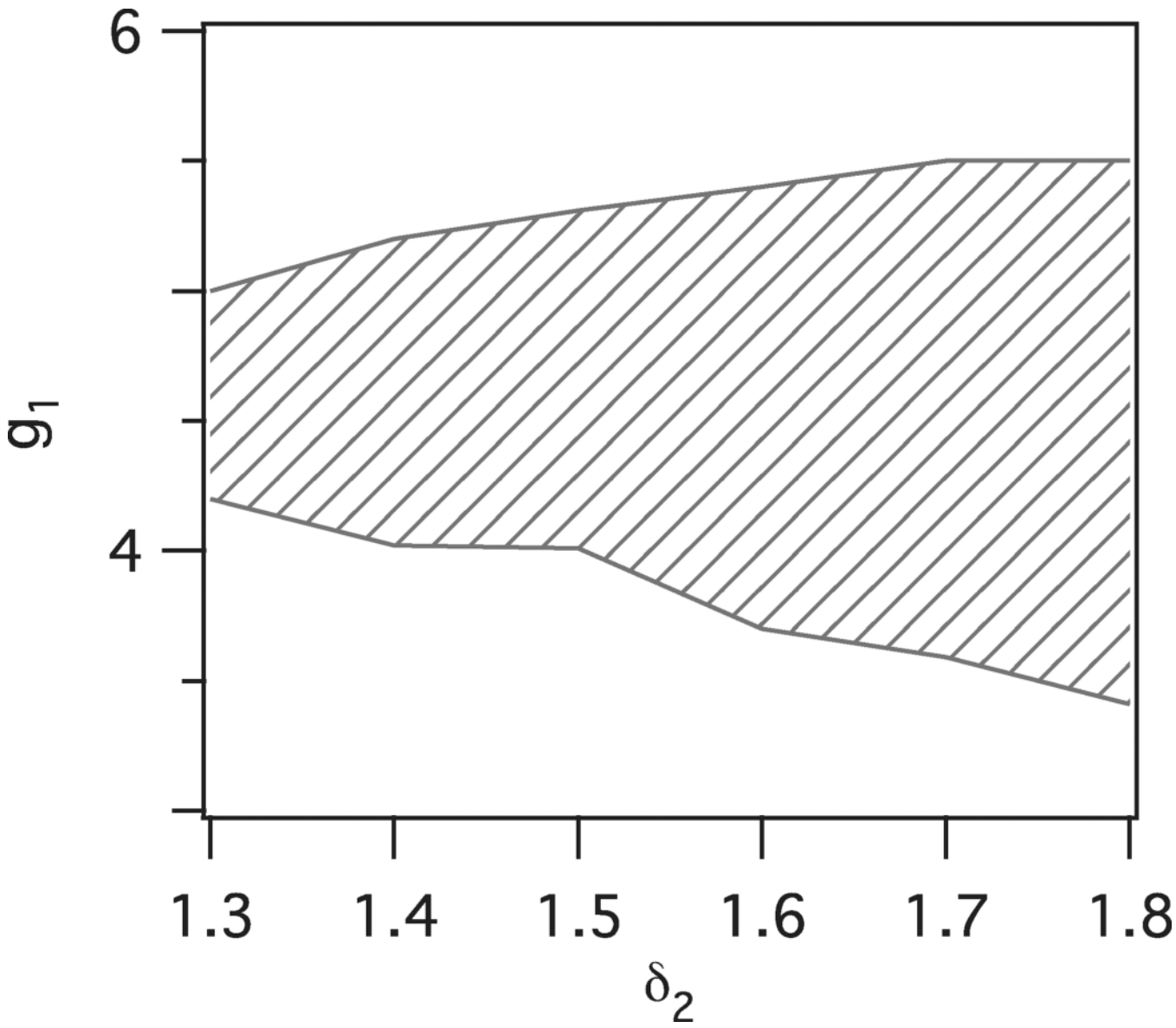


**Fig. 7.**
Stable single-pulse regime (shaded area) of the MMF laser as a function of $\delta_2$ (loss of the second mode) and $g_1$ (gain pumping strength of the first mode). As is expected, the operating regime increases as the MMF laser becomes more single mode in nature, i.e., the second mode content is more strongly filtered.

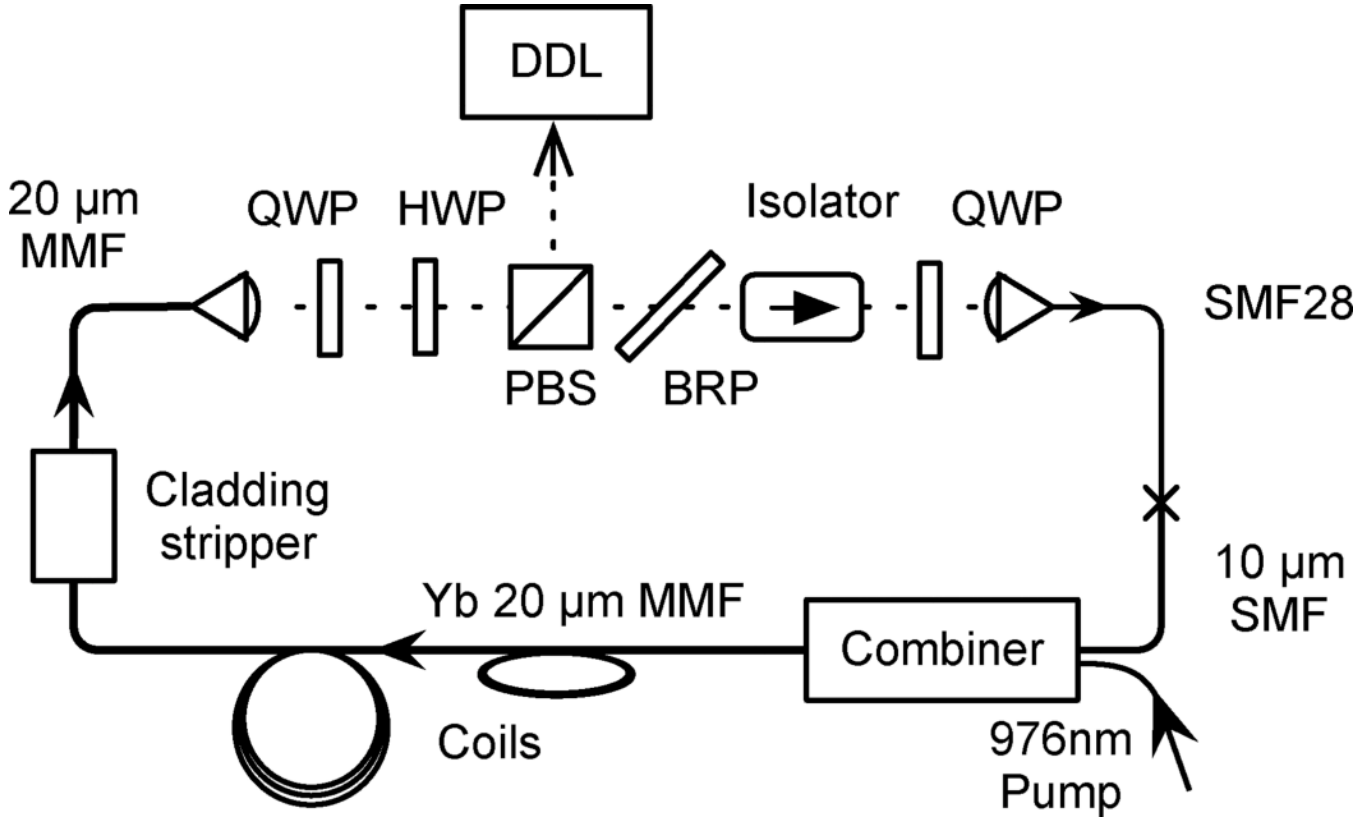


**Fig. 8.**
Step-index LMA ANDi laser setup. SMF/MMF: singlemode/multimode fiber, QWP/HWP: quarter/half waveplate, PBS: polarizing beam splitter, BRP: birefringent plate, and DDL: dispersive delay line.

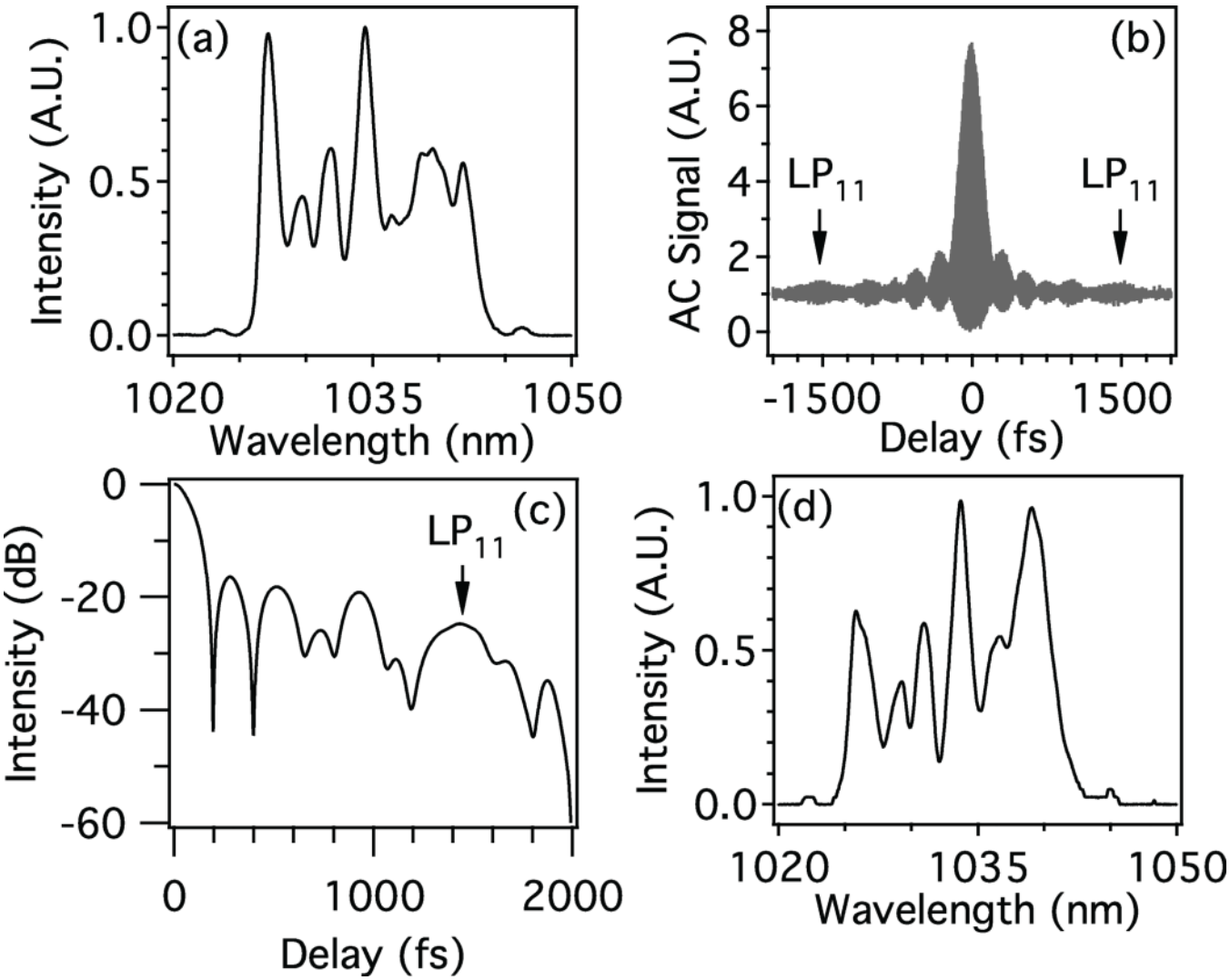


**Fig. 9.**

Mode-locked states of a step-index LMA ANDi laser without coiling: (a) spectrum and (b) dechirped interferometric AC of single pulsing state at 4.0 W of pump, (c) Fourier transform of (a) showing secondary pulse, and (d) double pulsing at 4.9 W pump.

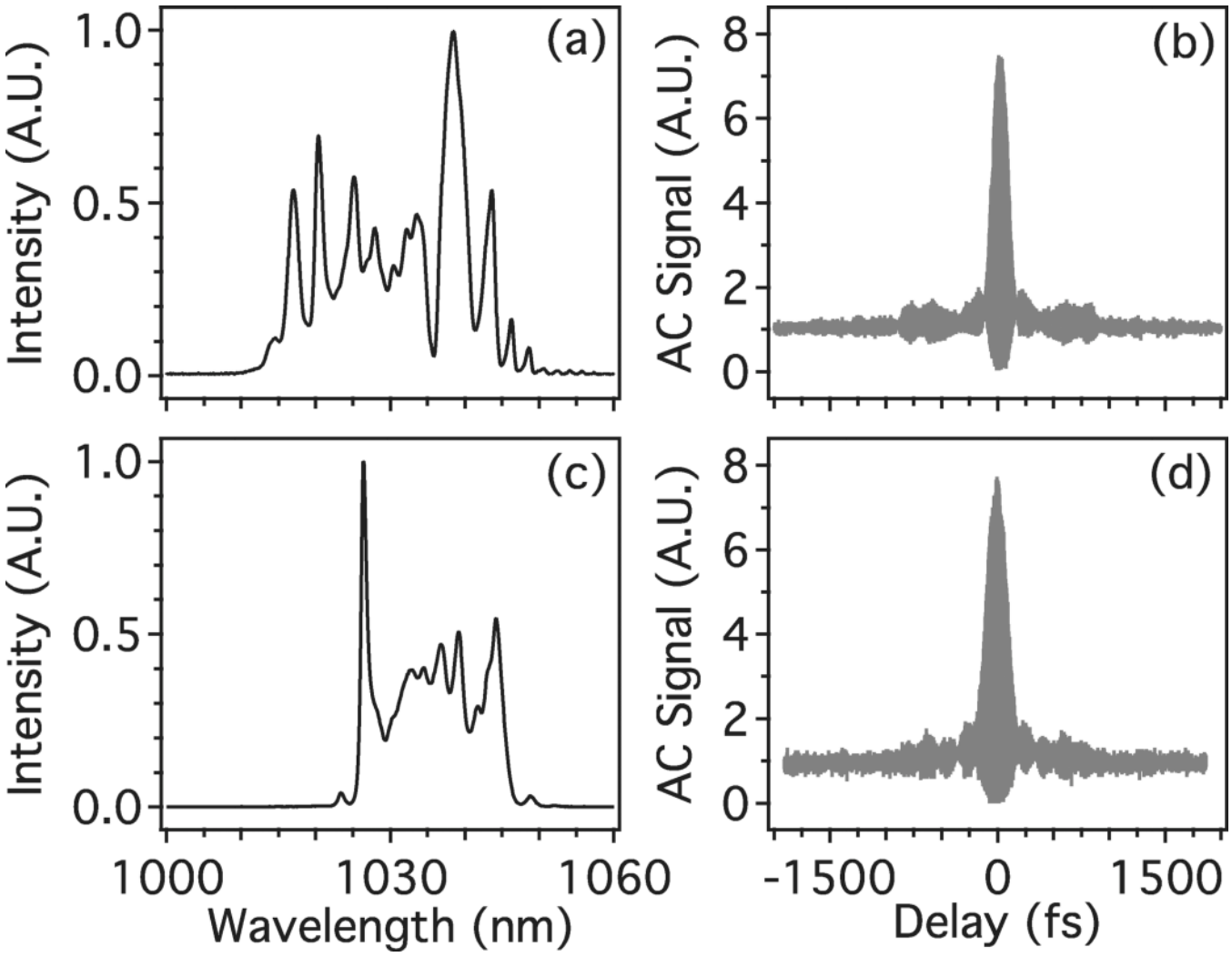


**Fig. 10.**
Mode-locked states of a step-index LMA ANDi laser with the gain fiber coiled to a diameter of 4 cm. Spectrum and dechirped interferometric AC using: (a) and (b) 15 nm filter, (c) and (d) 20 nm filter.

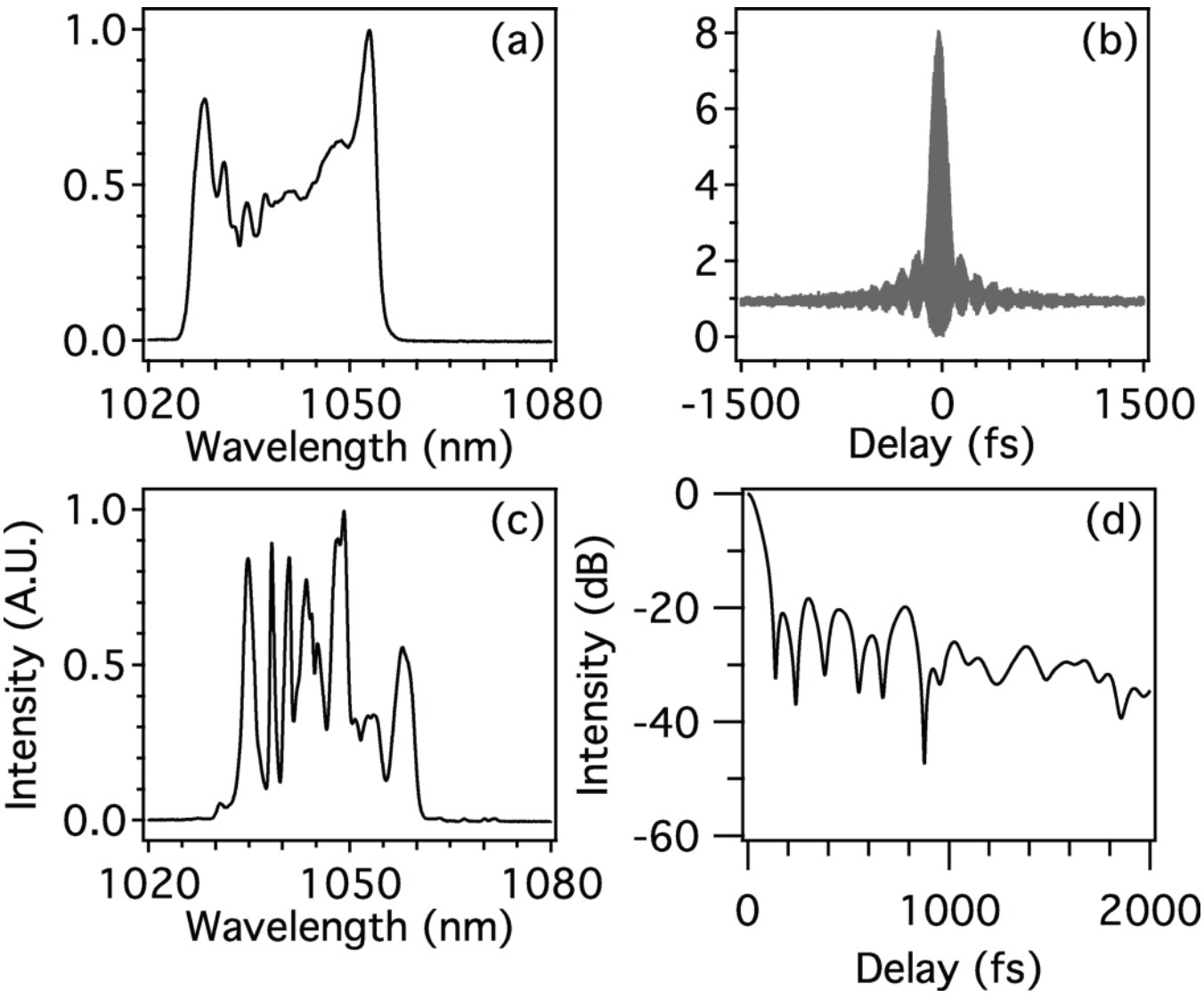


**Fig. 11.**

Mode-locked states of a LMA PCF based ANDi laser. (a) and (b) Spectrum and dechirped interferometric AC of the effectively single mode PCF. (c) and (d) Spectrum and its Fourier transform for the effectively multimode PCF.

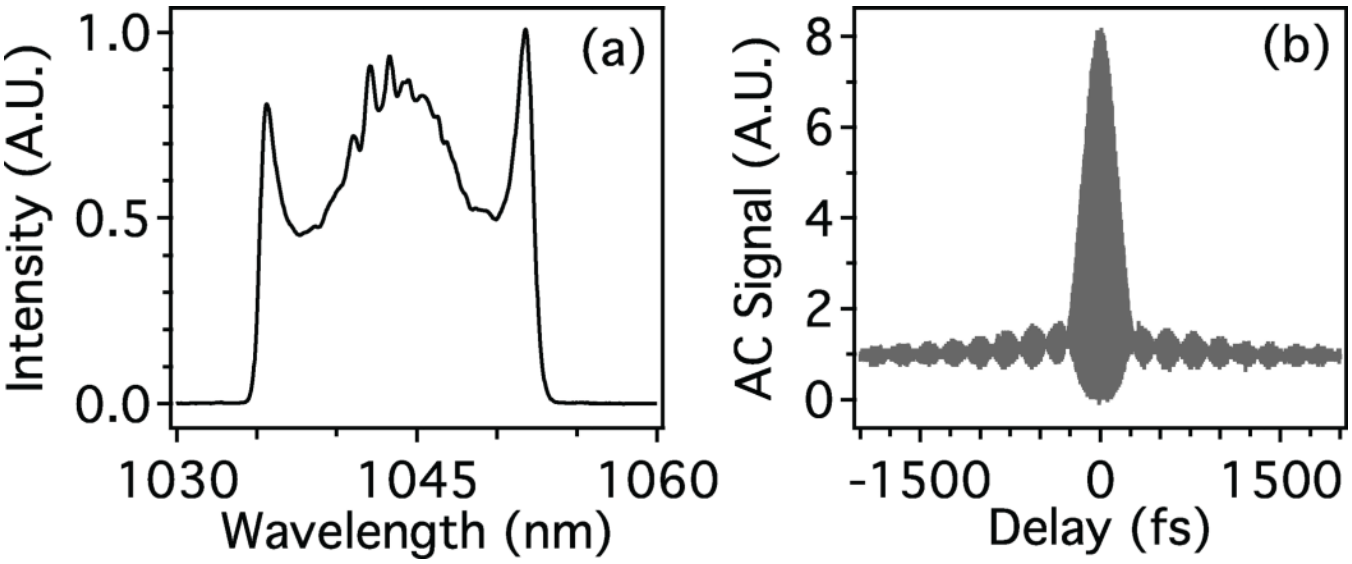


**Fig. 12.**
Mode-locked state of a LMA CCC fiber ANDi laser: (a) spectrum and (b) dechirped interferometric AC.